Molecular Cell
Article

RIG-I Forms Signaling-Competent Filaments in an ATP-Dependent, Ubiquitin-Independent Manner

Alys Peisley,[1,3,6] Bin Wu,[1,3,6] Hui Yao,[3,4] Thomas Walz,[2,5] and Sun Hur[1,3,*]
[1]Department of Biological Chemistry and Molecular Pharmacology
[2]Department of Cell Biology
Harvard Medical School, Boston, MA 02115, USA
[3]Program in Cellular and Molecular Medicine, Children's Hospital Boston, Boston, MA 02115, USA
[4]Department of Biochemistry and Molecular Biology, Nankai University, Tianjin 300071, China
[5]Howard Hughes Medical Institute, Chevy Chase, MD 20815-6789, USA
[6]These authors contributed equally to this work
*Correspondence: sun.hur@childrens.harvard.edu
http://dx.doi.org/10.1016/j.molcel.2013.07.024

SUMMARY

Retinoic acid-inducible gene 1 (RIG-I) and melanoma differentiation-associated protein 5 (MDA5) are paralogous receptors for viral double-stranded RNA (dsRNA) with divergent specificity. We have previously shown that MDA5 forms filaments upon viral dsRNA recognition and that this filament formation is essential for interferon signal activation. Here, we show that while RIG-I binds to a dsRNA end as a monomer in the absence of ATP, it assembles in the presence of ATP into a filament that propagates from the dsRNA end to the interior. Furthermore, RIG-I filaments directly stimulate mitochondrial antiviral signaling (MAVS) filament formation without any cofactor, such as polyubiquitin chains, and forced juxtaposition of the isolated signaling domain of RIG-I, as it would be in the filament, is sufficient to activate interferon signaling. Our findings thus define filamentous architecture as a common yet versatile molecular platform for divergent viral RNA detection and proximity-induced signal activation by RIG-I and MDA5.

INTRODUCTION

Effective immune defense against viral infection depends upon efficient detection of viral RNAs by innate immune receptors. Retinoic acid-inducible gene 1 (RIG-I) and its paralog, melanoma differentiation-associated protein 5 (MDA5), represent one such family of receptors that recognize viral double-stranded RNAs (dsRNAs) in the cytoplasm and activate antiviral signaling pathways in a wide range of cell types (Kato et al., 2011). We, and others, have previously shown that MDA5 cooperatively forms a filament along the length of dsRNA (Berke and Modis, 2012; Peisley et al., 2011) and that this filament formation is important for high-affinity interaction with dsRNA and oligomerization of its signaling domain, the tandem caspase activation recruitment domain (2CARD) (Peisley et al., 2012; Wu et al., 2013). Oligomerized 2CARD activates the downstream signaling adaptor molecule, mitochondrial antiviral signaling (MAVS), by promoting its transition from a monomer to filamentous state (Wu et al., 2013). MAVS filaments, in turn, recruit further downstream signaling molecules, such as TNF receptor-associated factor 2 (TRAF2), TRAF3, and TRAF6, and activate the interferon (IFN)-α/ IFN-β signaling pathways (Hou et al., 2011).

Unlike MDA5, oligomerization of its paralogous receptor, RIG-I, has been controversial. An atomic force microscopy study suggested that RIG-I also forms filaments along dsRNA (Binder et al., 2011). However, structural and biochemical analyses revealed that RIG-I binds to the dsRNA end as a monomer with little cooperativity (Jiang et al., 2011; Kowalinski et al., 2011; Luo et al., 2011), and that the C-terminal domain (CTD) caps the RNA end, which is incompatible with filament formation (Lu et al., 2010; Wang et al., 2010). Furthermore, RIG-I recognizes short dsRNA with a strong preference for the 5′-triphosphate group (5′ppp) and blunt ends that are expected in the genomic RNAs of several negative-strand viruses or its defective interfering particles (Baum et al., 2010; Schlee et al., 2009). Oligomerization of isolated RIG-I 2CARD was instead shown to require K63-linked polyubiquitin chains (K63-Ub_n) and was proposed to be required for MAVS filament formation and IFN-α/IFN-β signal activation (Jiang et al., 2012). However, the Lys residue (K172 in human RIG-I) critical for K63-Ub_n conjugation or binding is poorly conserved in vertebrates, and its mutation into Arg (K172R) was reported to have little effect on the IFN signaling activity of RIG-I during Sendai virus (SeV) infection (Shigemoto et al., 2009), suggesting the possibility of an alternative oligomerization and signaling mechanism for RIG-I.

Like MDA5, RIG-I contains a DExD/H motif helicase domain and displays dsRNA-dependent ATP hydrolysis activity, which in RIG-I was shown to confer its ability to translocate along dsRNA (Myong et al., 2009) and to be important for IFN signaling (Bamming and Horvath, 2009; Yoneyama et al., 2004). Here, we demonstrate that full-length RIG-I forms signaling-competent filamentous oligomers in a manner dependent on ATP hydrolysis, but independent of K63-Ub_n, and that this filament can directly activate MAVS without polyubiquitin chains.

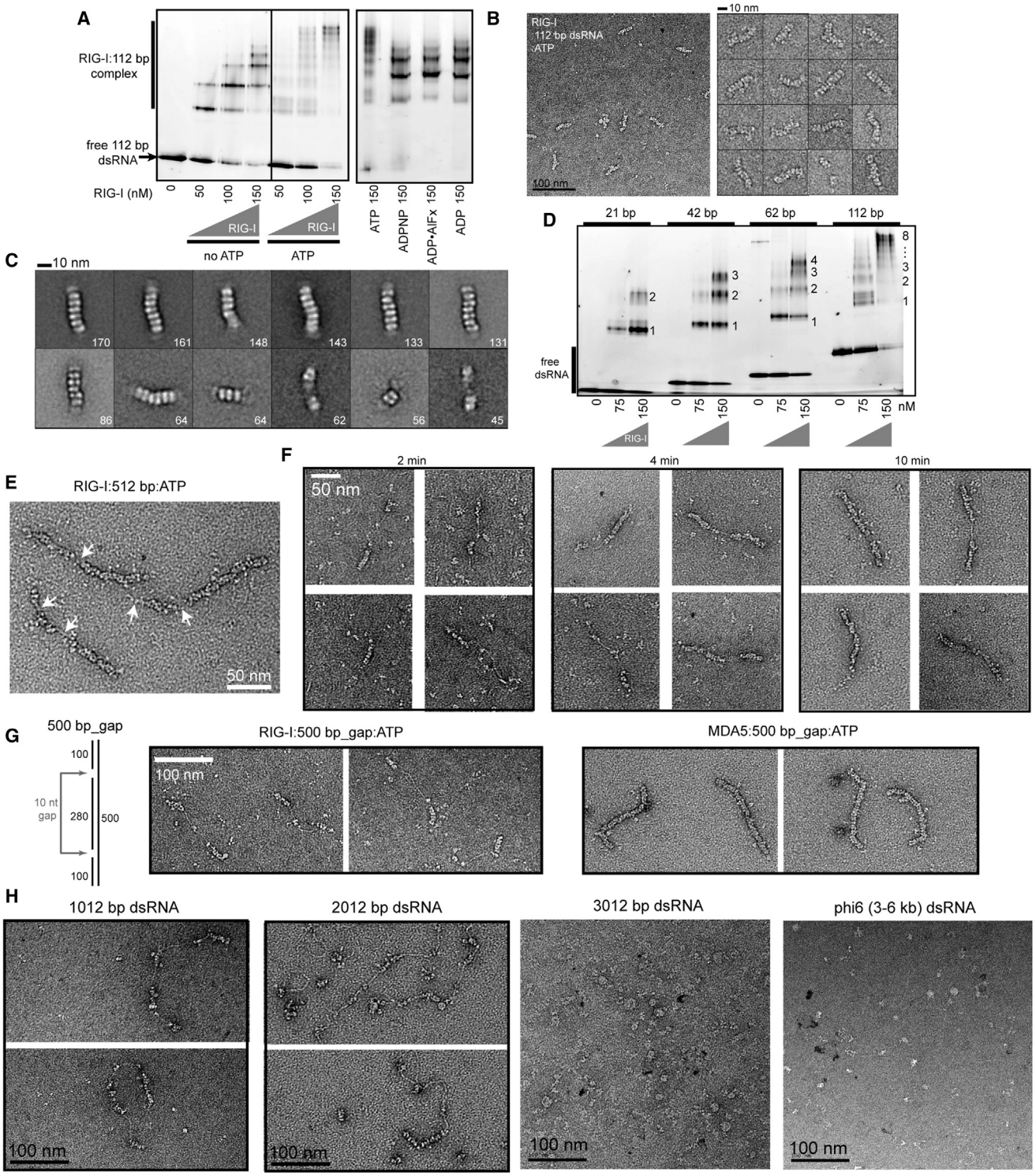

Figure 1. RIG-I Assembles into Filaments along dsRNA during ATP Hydrolysis

(A) EMSA of RIG-I on 112 bp dsRNA with and without 1 mM ATP and ATP analogs, stained with SYBR Gold. Unless mentioned otherwise, all dsRNAs contain 5′ppp and the blunt end throughout the paper.

(B) Representative EM image of RIG-I filaments formed with RIG-I (200 nM), 112 bp dsRNA (0.66 μg/ml, 10 nM), and ATP (1 mM) followed by quenching with ADP•AlF_x prior to sample preparation. See Figures S1B–S1D for the RIG-I:dsRNA complex without ATP or without ADP•AlF_x quenching or the catalytic mutant K270A in complex with dsRNA and ATP.

(legend continued on next page)

RESULTS

RIG-I Assembles into Filamentous Oligomers Near dsRNA Termini Only upon ATP Hydrolysis

In our effort to understand the role of ATP hydrolysis in RIG-I functions, we compared the complex formation of RIG-I and a 112 bp dsRNA with 5′ppp and the blunt end in the presence and absence of ATP. An electrophoretic mobility shift assay (EMSA) revealed that the complex formed with ATP migrates slower than those formed without ATP or with nonhydrolyzable ATP analogs (Figure 1A). Electron microscopy (EM) showed that the RIG-I:112 bp dsRNA complex formed with ATP, but not without ATP, has a filamentous architecture (Figures 1B and S1C available online). Consistent with the role of ATP hydrolysis in filament formation, a catalytic mutant, K270A, did not form filaments with ATP (Figure S1D). The importance of the helicase domain and lack of requirement for CARD domains in filament assembly was revealed by a 2CARD deletion mutant (Δ2CARD) that also formed filaments (Figure S1E).

Averages of full-length RIG-I filaments showed a segmented filament structure (Figure 1C) similar to that of the MDA5 filament (Peisley et al., 2011). Each segment is ~9–10 nm wide and ~4–5 nm thick, in agreement with the crystal structure of the ring-shaped RIG-I monomer bound to dsRNA (Jiang et al., 2011; Kowalinski et al., 2011; Luo et al., 2011). EMSA revealed 2, 3, 4–5, and ~8 bands of complexes formed with 21, 42, 62, and 112 bp dsRNAs, respectively (Figure 1D), suggesting that each monomer occupies ~14 bp, with the exception of the end-capping monomer, which occupies ~10 bp (Jiang et al., 2011; Kowalinski et al., 2011; Luo et al., 2011). This is in contrast to the RIG-I:dsRNA complex formed without ATP, where 112 bp dsRNA can accommodate up to ~5 RIG-I molecules even under the saturating condition (Figures S1C).

Compared to MDA5 filaments (Peisley et al., 2012; Peisley et al., 2011), RIG-I filaments showed more heterogeneous length distribution, with some displaying a dumbbell shape (Figure 1C). On 512 bp dsRNA, RIG-I filaments frequently contained gaps in the dsRNA interior, with the continuous stretch of the filament rarely exceeding ~100 nm (Figure 1E). These gaps were observed even with an excess amount of RIG-I, suggesting an intrinsic limitation in filament propagation. EM visualization of filament propagation intermediates often showed small filament fragments near dsRNA ends (Figure 1F). Additionally, introduction of single-stranded RNA (ssRNA) gaps 100 bp away from both ends of dsRNA resulted in only short stretches (~30–40 nm, equivalent to ~100 bp) of RIG-I filaments near the dsRNA ends (Figure 1G), suggesting that filaments propagate from the dsRNA end to the interior. This differed from MDA5 filaments, which showed full coverage over the entire dsRNA length with sharp kinks near the site expected for the gap (Figure 1G), in agreement with its nucleation on the dsRNA interior (Peisley et al., 2012).

Filament formation of RIG-I on longer dsRNAs (>1 kb) was less efficient than on shorter (<500 bp) RNAs. RIG-I filaments formed on in vitro transcribed 1,012 and 2,012 bp dsRNAs showed filament fragments no longer than ~100 nm, often near the dsRNA ends (Figure 1H). Interior filaments were occasionally observed, which may reflect the ability of RIG-I molecules or filaments to translocate from the dsRNA end to the interior. With in vitro transcribed 3,012 bp dsRNA and 3–6 kb phi6 phage dsRNA, filaments were not observed at the same mass concentration (Figure 1H), whereas small filaments (<100 nm) were observed when increasing the RNA concentration to match the molar concentration to that of the 112 bp dsRNA (Figure S1H, ~10 nM). Note that the amount of dsRNA ends remains constant regardless of the dsRNA length at the same molar concentration, whereas it is anticorrelated with dsRNA length at the same mass concentration. These results thus suggest that the availability of the dsRNA end is important for efficient filament formation and rationalize the observed preference of RIG-I for short dsRNAs at the same mass, but not molar, concentration (Baum et al., 2010; Binder et al., 2011).

Assembly of RIG-I Filaments Depends on 5′ppp and a Blunt End and Is Inhibited by Internally Modified Nucleotides

We next examined the sensitivity of filament formation to chemical and structural features of dsRNA ends, such as 5′ hydroxyl group (5′OH) and 5′ and 3′ overhangs, which are known to suppress RNA recognition by RIG-I (Schlee et al., 2009) (Figure S2A). We generated three end variants of 112 bp dsRNA by removing 5′ppp using calf intestinal phosphatase (CIP) or by placing a 20 nt overhang at either the 5′ or 3′ end of 112 bp dsRNA ends and formed the complex with RIG-I in the presence of ATP. By EMSA and EM, we found that both removal of 5′ppp and addition of 5′ or 3′ overhang reduced filament formation efficiency, with more significant effects observed with overhangs (Figure 2A). The dsRNA with a single 5′ppp supported filament formation (Figure S2B), suggesting that a single dsRNA end is sufficient for filament formation. The impact of alterations in the dsRNA end on filament formation supports that filaments

(C) Representative class averages of RIG-I filaments formed on 112 bp dsRNA from (B). The number of particles in the individual averages is indicated at the bottom right corner.

(D) EMSA of RIG-I with 21, 42, 62, and 112 bp dsRNA in the presence of ATP (SYBR Gold stain). Numbers beside band positions indicate the number of RIG-I molecules assembled on dsRNA. See Figure S1F for the equivalent EMSA without ATP.

(E) EM images of RIG-I filaments formed on 512 bp dsRNA (0.66 μg/ml, 2 nM) as in (B). Arrows indicate unoccupied dsRNA stretches.

(F) EM images of RIG-I filament formation intermediates. Filaments were formed on 512 bp dsRNA as in (E) and quenched at indicated time points by ADP•AlF_x. See Figure S1G for time-dependent EMSA.

(G) EM images of RIG-I and MDA5 filaments formed on 500 bp dsRNA with 2 10 nt ssRNA gaps positioned 100 bp from dsRNA ends demonstrate differences in filament assembly mechanisms between RIG-I and MDA5. Filaments were formed as in (B).

(H) EM images of RIG-I filaments formed on in vitro transcribed 1,012, 2,012, and 3,012 bp dsRNAs (0.66 μg/ml) and phi6 dsRNAs (0.66 μg/ml), which contain a mixture of 2,948 bp, 4,063 bp, and 6,374 bp dsRNAs. As with in vitro transcribed dsRNAs, phi6 dsRNAs would contain 5′ppp and blunt ends due to the primer-independent replication mechanism of phi6 replicase (Makeyev and Grimes, 2004). See Figure S1H for filaments on 3 kb and phi6 dsRNA at higher RNA concentrations. See also Figure S1.

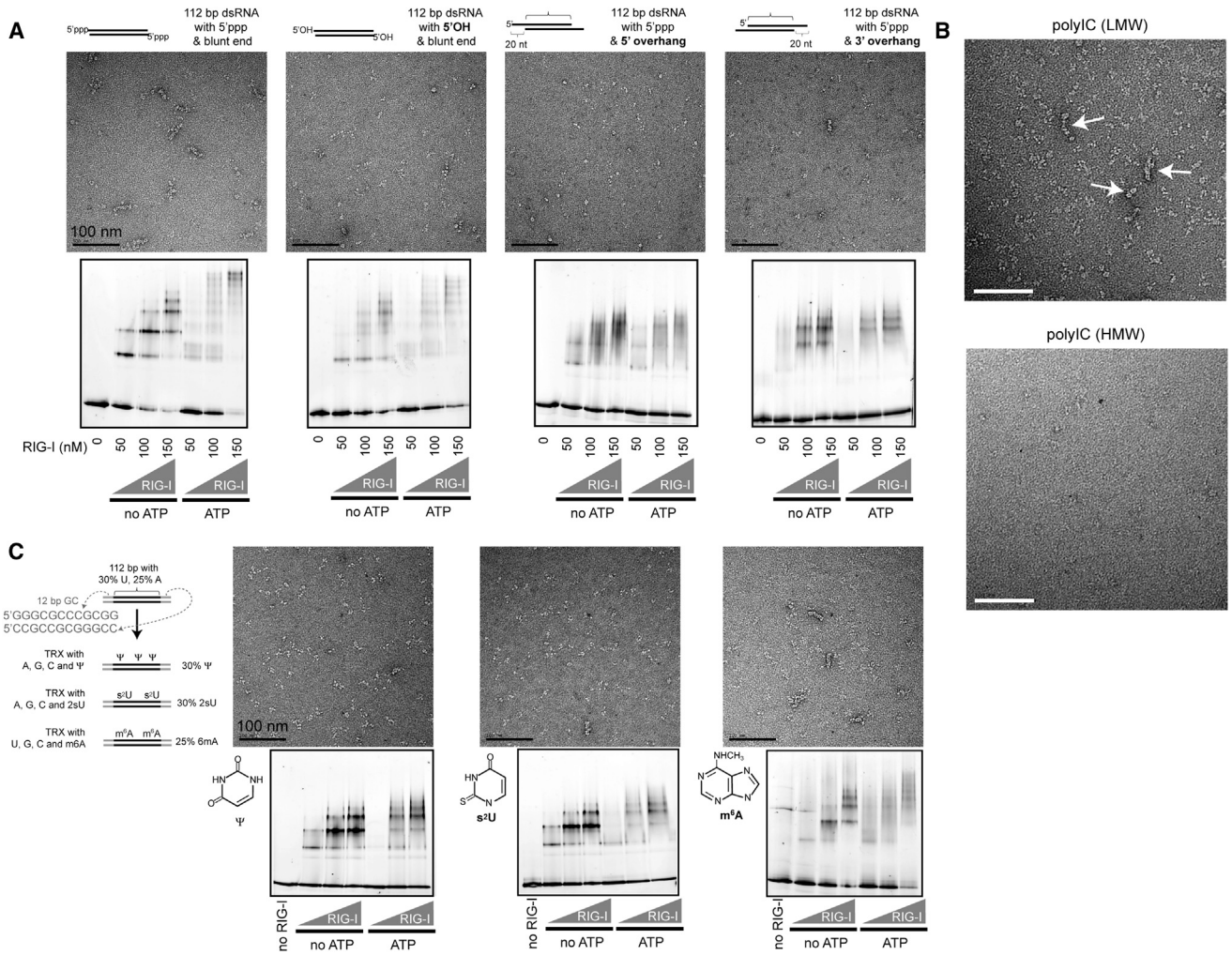

Figure 2. Assembly of RIG-I Filaments Depends on 5′ppp and a Blunt End and Is Inhibited by Modified Nucleotides

(A) EM images of RIG-I with dsRNA without 5′ppp or with 5′ or 3′ overhangs in the presence of ATP. Shown below the EM images are the gel images of RIG-I EMSA with and without ATP.

(B) EM images of RIG-I filaments formed on LMW and HMW polyIC (0.66 μg/ml) with ATP.

(C) Left: schematic of preparation of 136 bp dsRNA with Ψ, s^2U, and m^6A, which were incorporated into RNA during transcription in the absence of their respective unmodified nucleotide (i.e., uridine triphosphate [UTP] or ATP), resulting in complete replacement of U (30% of the total sequence) by Ψ and s^2U, and A (25%) by m^6A. EM images of RIG-I in complex with dsRNA containing modified nucleotides in the presence of ATP. Shown below the EM images are the gel images of RIG-I EMSA with and without ATP. See also Figure S2.

propagate from the dsRNA end to the interior. The 5′ppp and blunt end, however, do not appear to be the absolute requirement for RIG-I filaments, as we observed short filaments, albeit infrequently, with low-molecular-weight (LMW) polyinosinic-polycytidylic acid (polyIC), a dsRNA mimic without 5′ppp (Figure 2B). No such filaments were observed with high-molecular-weight (HMW) polyIC, consistent with the previous observation that RIG-I prefers LMW to HMW polyIC (Kato et al., 2008). These observations suggest that, while 5′ppp and blunt ends strongly promote filament formation on dsRNA, additional mechanisms may exist to explain RIG-I filament formation on polyIC.

To examine the importance of internal RNA regions, we generated three dsRNAs containing pseudouridine (Ψ), 2-thiouridine (s^2U), and N6-methyladenosine (m^6A), modified nucleotides that are often observed in cellular RNAs and do not affect the base-pairing ability of the nucleotides (Davis, 1998; Horowitz et al., 1984). These modified nucleotides were incorporated into the duplex interior during transcription without affecting the terminal 12 bp, which is composed only of G or C (Figure 2C). Filament formation was suppressed by these modifications, as evidenced by reduced mobility shift by EMSA and smaller oligomer size by EM (Figure 2C). This result suggests that RIG-I filament formation is not only sensitive to the dsRNA end features, but also to modified nucleotides throughout the body of dsRNA.

To dissect the importance of dsRNA end and ATP hydrolysis for filament nucleation versus propagation, we performed pulse-chase experiments in which RIG-I filaments were partially formed with pulse RIG-I (labeled with Alexa 488) and then

extended with chase RIG-I (labeled with Alexa 647). Between pulse and chase, we added RIG-I CTD or ADP•AlF_x to block RNA end or ATP hydrolysis, respectively, during filament extension with chase RIG-I (Figure S2D). Using EMSA and EM, we found that both CTD and ADP•AlF_x suppressed filament propagation with chase RIG-I (Figures S2C and S2D), suggesting that dsRNA ends and ATP hydrolysis are continuously required for both filament nucleation and propagation. This result is consistent with a model in which filaments are formed through sequential recruitment of individual RIG-I molecules to the dsRNA end and their subsequent movement to the dsRNA interior.

RIG-I Filaments Induce MAVS Filament Formation in the Absence of Polyubiquitin Chains

While the signaling activity of isolated 2CARD depends on K63-Ub_n, signaling by full-length RIG-I filaments appears to be independent of K63-Ub_n, as mutation of K172 or all 6 Lys residues (99, 169, 172, 181, 190, and 193; 6KR) known to be essential for K63-Ub_n conjugation and binding (Gack et al., 2007; Zeng et al., 2010) altered the cellular IFN-β reporter activity of 2CARD, but not of full-length RIG-I upon stimulation with 112 bp dsRNA (Figure 3A). This is consistent with the previous observation that K172 in full-length RIG-I is dispensable for IFN-β signaling upon SeV infection (Shigemoto et al., 2009) and that five of the six Lys residues are poorly conserved (Figure S3A).

To more directly examine whether RIG-I filaments can activate MAVS in the absence of K63-Ub_n, we used the MAVS filament formation assay, in which the monomer-to-filament transition of purified MAVS CARD fused to SNAP (CARD-S) was monitored by native gels and EM (Figure 3B) (Wu et al., 2013). We have previously shown that recombinant MAVS CARD-S purified from *E. coli* exists as short filaments and requires chemical refolding to obtain monomeric CARD-S. Refolded monomeric CARD-S recapitulates MAVS in mitochondria as it rapidly extended the seed filaments (Figure 3C), a self-perpetuating property previously reported for native MAVS on mitochondrion (Hou et al., 2011). In addition, the filament formation propensity of CARD-S in vitro correlated with the signaling activity of full-length MAVS in cells (Figures 3D and 3E), suggesting that CARD-S filament formation can be used as a direct measure of the signaling capability of RIG-I. In agreement with the results from cellular assays (Figure 3A), isolated 2CARD required K63-Ub_n to stimulate MAVS filament formation (Figure 3F). However, full-length RIG-I, but not Δ2CARD, was able to stimulate MAVS filament formation in the absence of K63-Ub_n when bound to 112 bp dsRNA with ATP. No MAVS stimulation was observed without ATP or RNA in the absence of K63-Ub_n (Figures 3G and S3E).

To further compare the signal activation mechanism of isolated 2CARD with K63-Ub_n and RIG-I filament without K63-Ub_n, we examined three surface mutations in 2CARD, E35A/E36A, E137A/E138A, and D21A, which disrupted the oligomerization (Figures 3I and S3G) and MAVS stimulatory activity (Figure 3F) of isolated 2CARD. We found that the same mutations in full-length RIG-I also disrupted K63-Ub_n-independent MAVS stimulatory activity of RIG-I filaments in vitro (Figure 3J) and its signaling activity in cells (Figure 3K). These results suggest that the same surface of 2CARD is involved in K63-Ub_n-dependent oligomerization of isolated 2CARD and K63-Ub_n-independent signaling activity of the RIG-I filament. Note that the full-length E35A/E36A mutant partially retained MAVS stimulatory activity in the presence of both K63-Ub_n and ATP, but not with K63-Ub_n or ATP alone, consistent with the lack of MAVS stimulatory activity of isolated 2CARD (E35A/E36A) with K63-Ub_n (Figure 3F). These results suggest the synergistic relationship between the ubiquitin- and filament-dependent signaling mechanisms of full-length RIG-I and also rationalize the residual signaling activity of full-length E35A/E36A in cells (Figure 3K).

In support of the importance of RIG-I filaments in Ub-independent MAVS stimulation, an excess amount of RNA, which disintegrated the RIG-I filament, decreased the efficiency of MAVS stimulation (Figure 4A). Additionally, RIG-I bound to modified dsRNAs with ATP did not stimulate MAVS filament formation in the absence of K63-Ub_n (Figure S4A). Furthermore, RIG-I filaments on 112 and 62 bp dsRNAs, but not 42 and 21 bp dsRNAs, stimulated MAVS without K63-Ub_n in the presence of ATP (Figures 3G and 4B). As 21, 42, 62, and 112 bp dsRNAs can accommodate 2, 3, 4–5, and ~8 RIG-I molecules, respectively (Figure 1D), this result suggests that a minimum of four RIG-I molecules are required for MAVS stimulation without K63-Ub_n, which parallels the previous finding of tetramerization of isolated 2CARD upon interaction with K63-Ub_n (Jiang et al., 2012). Finally, mutations of K462/E464 and Q336/N340 on the head and tail surface, respectively, of the putative monomer:monomer interface in the model of a RIG-I filament had an additive, negative impact on filament formation and the signaling activity of RIG-I (Figure 4C).

Visual inspection of MAVS filaments by EM showed that RIG-I was often present at the end of the MAVS filament, suggesting end nucleation and unidirectional propagation of MAVS filaments (Figure 4D). Interestingly, at higher RIG-I concentrations, RIG-I formed clusters near MAVS filament termini (Figure 4D), which were not observed without MAVS or RIG-I filaments (Figure 3F), suggesting that clustering of RIG-I is a result of interactions between RIG-I filaments and MAVS or MAVS filaments.

K63-Linked Polyubiquitin Chains Can Act Both Parallel to and Synergistically with RIG-I Filaments in MAVS Stimulation

In contrast to the situation without K63-Ub_n, in the presence of K63-Ub_n, RIG-I bound to dsRNA induced MAVS filament formation without ATP and regardless of the dsRNA length or modifications (Figures 4B, S4A, and S4C). In cells, s^2U-modified dsRNA showed even higher stimulatory activity than unmodified dsRNA (Figure S4B), despite reduced filament formation observed in vitro (Figure 2C). These results suggest that filament formation is not absolutely required for signal activation in the presence of K63-Ub_n. The dispensable nature of ATP in MAVS stimulation in the presence of K63-Ub_n further supports a previous model that RNA binding triggers 2CARD release, which then oligomerizes via K63-Ub_n without the requirement of prearranged proximity. Consistently, K270A also stimulated MAVS without ATP in the presence of K63-Ub_n (Figure S4D). However, the ability of K270A to stimulate MAVS was inhibited by ATP (Figure S4D), presumably due to ATP binding (Figure S4E), which rationalizes its lack of signaling activity in cells

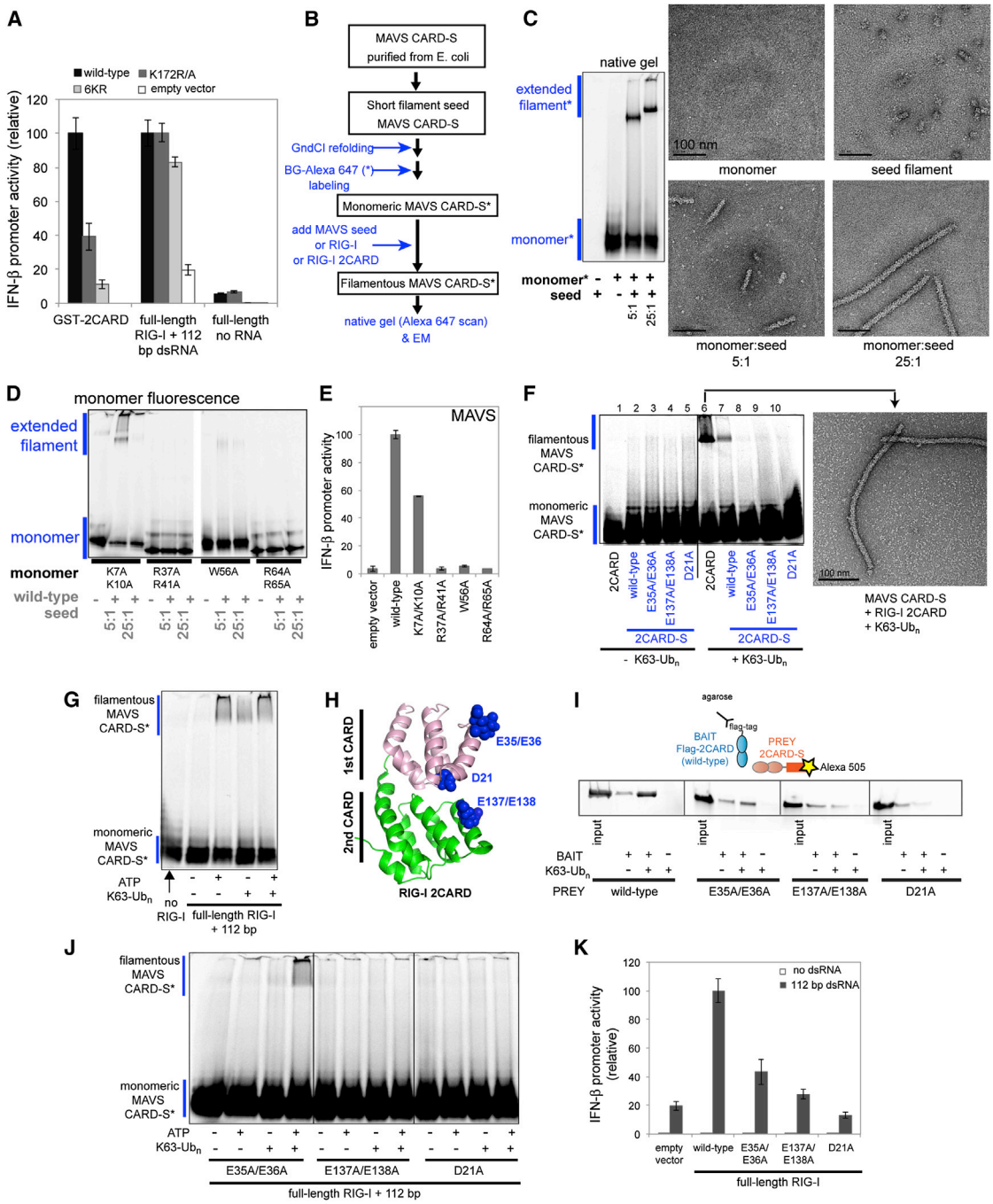

Figure 3. RIG-I Filaments Stimulate MAVS Filament Formation Independently of K63-Ub$_n$

(A) IFN-β reporter activity of wild-type, K172R, and 6KR of isolated 2CARD (fused to glutathione S-transferase [GST]), and wild-type, K172A, and 6KR of full-length RIG-I stimulated with 5′ppp, blunt-ended 112 bp dsRNA in 293T cells. Level of stimulation was normalized against the wild-type activity (mean ± SD, n = 3).

(B) Schematic of the MAVS filament formation assay. MAVS CARD-S expressed in *E. coli* existed as short filaments, which were refolded using guanidinium hydrochloride (GndCl) to obtain monomeric CARD-S. Refolded monomeric CARD-S was labeled with Alexa 647 (CARD-S*) to monitor its filament formation on native gels in Figures 3 and 4.

(C) MAVS CARD-S filament seed extension assay as examined by EMSA and EM. Monomeric CARD-S* (10 μM) was incubated with seed filaments purified from *E. coli* at indicated mass ratios.

(D) Filament extension by mutant MAVS CARD-S*. The ability of monomeric, mutant CARD-S* to extend the wild-type seed filament was monitored by EMSA using the CARD-S* fluorescence. See Figure S3C for overlaid fluorescence images of seed filaments and monomeric CARD-S*.

(E) IFN-β reporter activity of wild-type and mutant MAVS (mean ± SD, n = 3).

(legend continued on next page)

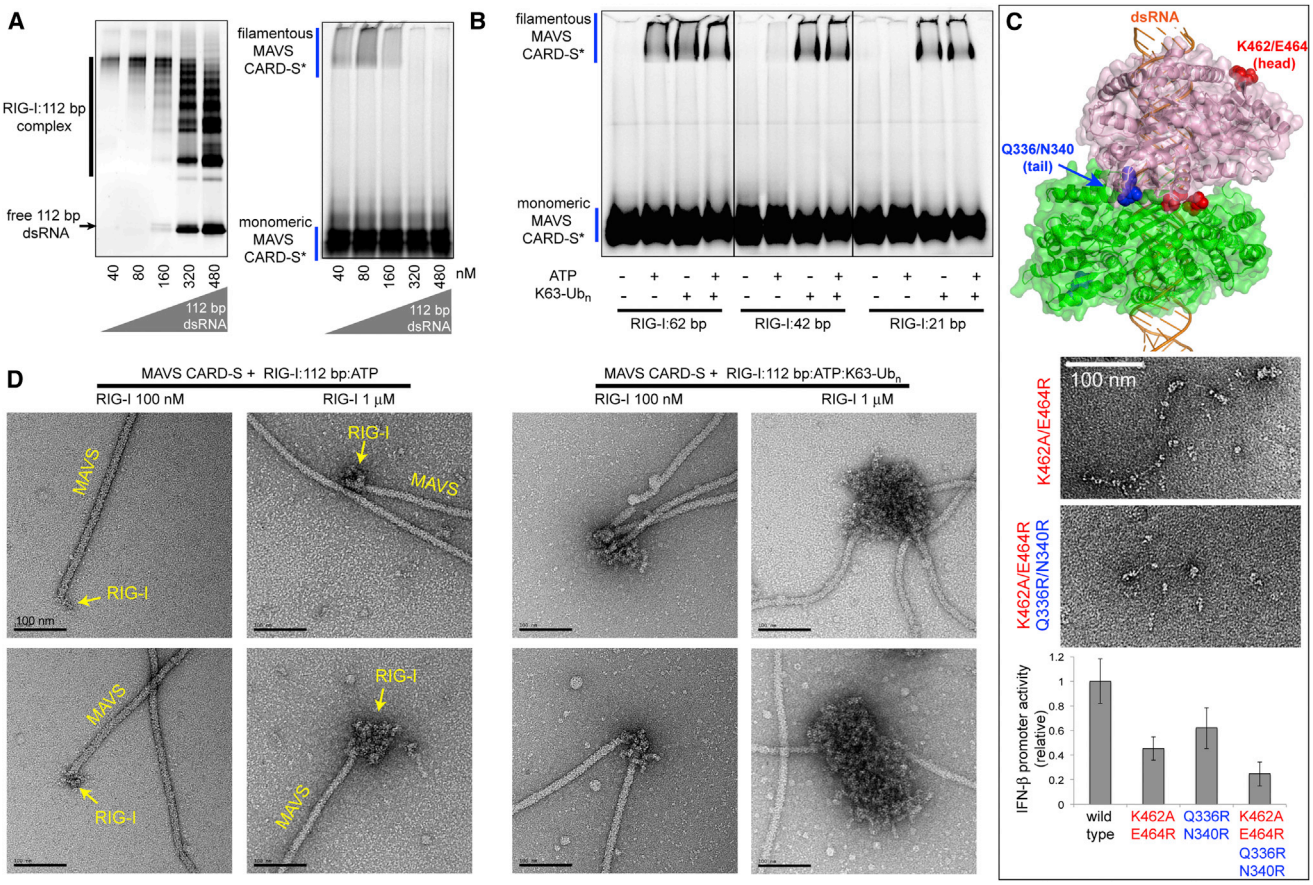

Figure 4. Importance of RIG-I Filament Assembly for the Stimulation of MAVS Filament Formation

(A) Dependence of RIG-I filament formation (left, SYBR Gold stain) and MAVS CARD-S filament stimulation (right, Alexa 647 fluorescence on CARD-S) on the concentration of 112 bp dsRNA in the presence of ATP without K63-Ub$_n$.

(B) MAVS CARD-S filament formation stimulated by RIG-I in complex with 21, 42, and 62 bp dsRNAs with and without ATP or K63-Ub$_n$.

(C) A model of the RIG-I filament generated by head-to-tail stacking of monomeric RIG-I molecules bound to dsRNA (PDB ID: 3TMI) while imposing dsRNA continuity and a periodicity of 14 bp. This model resembles the experimentally validated model of the MDA5 filament (Berke et al., 2012; Wu et al., 2013) and predicts that K462/E462 and Q336/N340 in the head and tail surface, respectively, are involved in monomer:monomer contacts. These residues are >15 Å away from the dsRNA. Below are the representative EM images of K462/E462 and K462/E462/Q336/N340 bound to 512 bp dsRNA with ATP. At the bottom is the IFN-β reporter activity of wild-type and mutants containing K462A/E464R and/or Q336R/N340R upon stimulation with 5′ppp, blunt-ended 112 bp dsRNA in 293T cells (mean ± SD, n = 3).

(D) Representative EM images of MAVS CARD-S filaments induced by RIG-I oligomers with and without K63-Ub$_n$. Unidirectional MAVS filament propagation is indicated by the presence of nucleation centers containing RIG-I at one end of a MAVS filament. See also Figure S4.

(Yoneyama et al., 2004). Parallel to the sensitivity of K270A to ATP, the ability of wild-type RIG-I to stimulate MAVS in the presence of K63-Ub$_n$ was inhibited by ADP, but not by ATP, ADPNP, or ADP•AlF$_x$ (Figure S4F), suggesting the exquisite sensitivity of the 2CARD conformation to the ATP hydrolysis state and active site mutations.

(F) MAVS CARD-S filament formation stimulated by isolated RIG-I 2CARD or 2CARD conjugated to SNAP (2CARD-S) with and without K63-Ub$_n$. While SNAP reduces the 2CARD's ability to stimulate MAVS filament formation, possibly due to steric interference with oligomerization or interaction with K63-Ub$_n$ or MAVS, comparison of MAVS stimulatory activities of wild-type and mutant 2CARD remains valid. 2CARD surface mutations are indicated in (H). Right: EM image of the MAVS filament formed by stimulation with wild-type RIG-I 2CARD in the presence of K63-Ub$_n$ (lane 6).

(G) MAVS CARD-S filament formation stimulated by RIG-I:112 bp dsRNA complexes formed with and without ATP and K63-Ub$_n$. See Figure S3D for the gel image obtained using fluorescein conjugated to RIG-I. See also Figure S3E for MAVS stimulated by RIG-I without dsRNA or Δ2CARD filaments.

(H) Mutations of 2CARD mapped onto a homology model of human RIG-I based on the structure of duck RIG-I (Protein Data Bank ID: 4A2W). The homology model was generated using the program Rosetta (Leaver-Fay et al., 2011).

(I) SDS-PAGE analysis of pull-downs of wild-type and mutant RIG-I 2CARD-S using wild-type Flag-2CARD with and without K63-Ub$_n$. The gel images were obtained using Alexa 505 conjugated to 2CARD-S. See also Figures S3F and S3G for native gel analysis of K63-Ub$_n$-mediated 2CARD oligomerization.

(J) MAVS CARD-S stimulated by mutant RIG-I bound to 112 bp dsRNA with and without ATP and K63-Ub$_n$.

(K) IFN-β reporter activity of wild-type and mutant RIG-I stimulated by 112 bp dsRNA (mean ± SD, n = 3). See also Figure S3.

Comparison of MAVS stimulatory activity at various concentrations of the RIG-I:dsRNA complex showed higher activity of the RIG-I:dsRNA complex with ATP and K63-Ub_n than with ATP or K63-Ub_n alone (Figure S4G). EM inspection of the MAVS filaments revealed more pronounced clustering of RIG-I with K63-Ub_n than without and branching of multiple MAVS filaments from a single RIG-I cluster (Figure 4D), suggesting a role of K63-Ub_n in signal amplification.

Induced Proximity of 2CARD Is Sufficient to Activate IFN Signaling in the Absence of K63-Linked Polyubiquitin Chains

To examine whether induced proximity of 2CARD within the RIG-I filament is important for MAVS stimulation, we fused isolated 2CARD to a zinc finger (ZF) domain of human Zif268, which specifically binds to the sequence GCGTGGGCG (Jamieson et al., 1996) (Figure 5A). To examine the K63-Ub_n-independent signaling activity, we used the 6KR mutant and measured the IFN-β promoter reporter activity in response to stimulation with DNA oligonucleotides containing 0–4 tandem copies of the Zif268 recognition sequence. In comparison to no DNA, addition of 47 bp DNA containing the 4 tandem ZF-binding sites (DNA-ZF4X) robustly stimulated (~20-fold) the signaling activity of 2CARD(6KR)-ZF, but not ZF or 2CARD(6KR) alone (Figure 5B). This signal activation was dependent on the ability of 2CARD to form oligomers, as E35A/E36A and E137A/E138A mutations disrupted the signaling activity of 2CARD(6KR)-ZF in the presence of DNA-ZF4X. Furthermore, a decrease in the number of ZF-binding sites gradually decreased the signaling activity (Figure 5B), suggesting that bridging of 2CARDs by DNA is important for signal activation. The moderate level of stimulation by DNA-ZF2X and DNA-ZF3X could indicate the possibility of the nonspecific bridging of 2CARD(6KR)-ZF in cells.

DISCUSSION

Ligand-induced receptor oligomerization is a common mechanism for signal activation. The RIG-I filament described here addresses the long-debated oligomeric architecture of full-length RIG-I and provides an explanation for the importance of ATP hydrolysis in signal activation. Our data support a model that RIG-I filament is formed by binding of individual RIG-I molecules to the dsRNA end and their subsequent translocation into the dsRNA interior and stacking along the translocation track (Figure 5C). The requirement of ATP hydrolysis in RIG-I filament formation rationalizes how previous analyses of RIG-I without ATP led to the notion of monomeric interaction between RIG-I and dsRNA (Jiang et al., 2011; Kowalinski et al., 2011; Luo et al., 2011). The crystal structures of RIG-I capping the dsRNA end (Jiang et al., 2011; Luo et al., 2011) thus represent RIG-I conformations prior to translocation and filament formation. The incompatibility of the end-capping structure of RIG-I with the filament architecture suggests that RIG-I must adopt a different conformation in the filament, likely resembling that of MDA5 wrapping around the dsRNA stem (Wu et al., 2013).

The RIG-I filament is distinct from the beads-on-a-string type of oligomers, which can be formed when an excess amount of RIG-I is incubated with dsRNA in the absence of ATP (Figure S1C). The importance of the direct contact between monomers within the ATP-driven filament was demonstrated by the observed reduction in filament formation and signaling activity upon disruption of the putative protein:protein interface (Figure 4C). The distinction between the RIG-I filament formed with ATP and multi-RIG-I:dsRNA complexes formed without ATP was further evidenced by our observations that RIG-I:dsRNA complexes formed without ATP displayed no filamentous oligomers by EM, lower packing density by EMSA, and lack of MAVS stimulatory activity. The ATP hydrolysis-driven translocation may allow tight packing of RIG-I monomers along dsRNA, whereas direct internal binding of RIG-I alone without translocation would lead to sparse and out-of-register placement of individual monomers on dsRNA.

Assembly of RIG-I filaments on dsRNA offers an elegant mechanism by which RIG-I utilizes dsRNA as a scaffold to bring multiple 2CARDs into proximity in a manner independent of ubiquitin chains (Figure 5C). Close proximity of 2CARDs within the filament appears to lead to formation of the same type of 2CARD oligomers as those induced by K63-Ub_n, as evidenced by the common requirement of four RIG-I 2CARD domains and the sensitivity to the identical surface residues for filament- and K63-Ub_n-dependent RIG-I signaling (Figure 3). The 50-residue-long linker (~15 nm assuming random coil) between 2CARD and the helicase domain is indeed long enough to allow direct contacts between 2CARDs that are six molecules apart (Figure 5C). The lack of requirement of K63-Ub_n for signal activation by the RIG-I filament is in contrast to the strict requirement of K63-Ub_n for isolated 2CARD (Gack et al., 2007) or RIG-I in complex with ssRNA (Zeng et al., 2010) or short dsRNA (<60 bp, Figure 4B), which do not support filament formation. These results suggest that filament- and ubiquitin-dependent signaling mechanisms act both in parallel and synergistically in recognition of a broad range of viral RNAs.

Previous studies showed that RIG-I preferentially recognizes the genome of defective interfering (DI) particles that contain an ~100 bp complementary region as opposed to the wild-type SeV genome with ~20 bp complementarity (Baum et al., 2010). The dsRNA structure of the SeV DI genome can support RIG-I filament formation, as the DI genome contains the perfectly complementary 5′ and 3′ termini (as a product of copy-back replication; Lazzarini et al., 1981), which can form a perfect duplex with 5′ppp and the blunt end. In support of the importance of the RIG-I filament in viral detection, the level of IFN stimulation by SeV and vesicular stomatitis virus (VSV) correlated with the length of the complementary region in the viral genome (Strahle et al., 2006; Sekellick and Marcus, 1982). Similarly, IFN stimulation by in vitro transcribed dsRNA (compared at the same molar concentrations) also increased with dsRNA length up to ~500 bp (Binder et al., 2011). As the concentration of the dsRNA end remains constant over different lengths of dsRNAs at the same molar concentration, this result cannot be explained by monomeric binding of RIG-I to the dsRNA end but is in agreement with the role of RIG-I filament in dsRNA detection.

How, then, can one reconcile the observed inefficiency of RIG-I in recognizing long (>~1–2 kb) dsRNAs when compared at the same mass concentration (Kato et al., 2008)? This is likely due to the limited availability of long dsRNA ends when

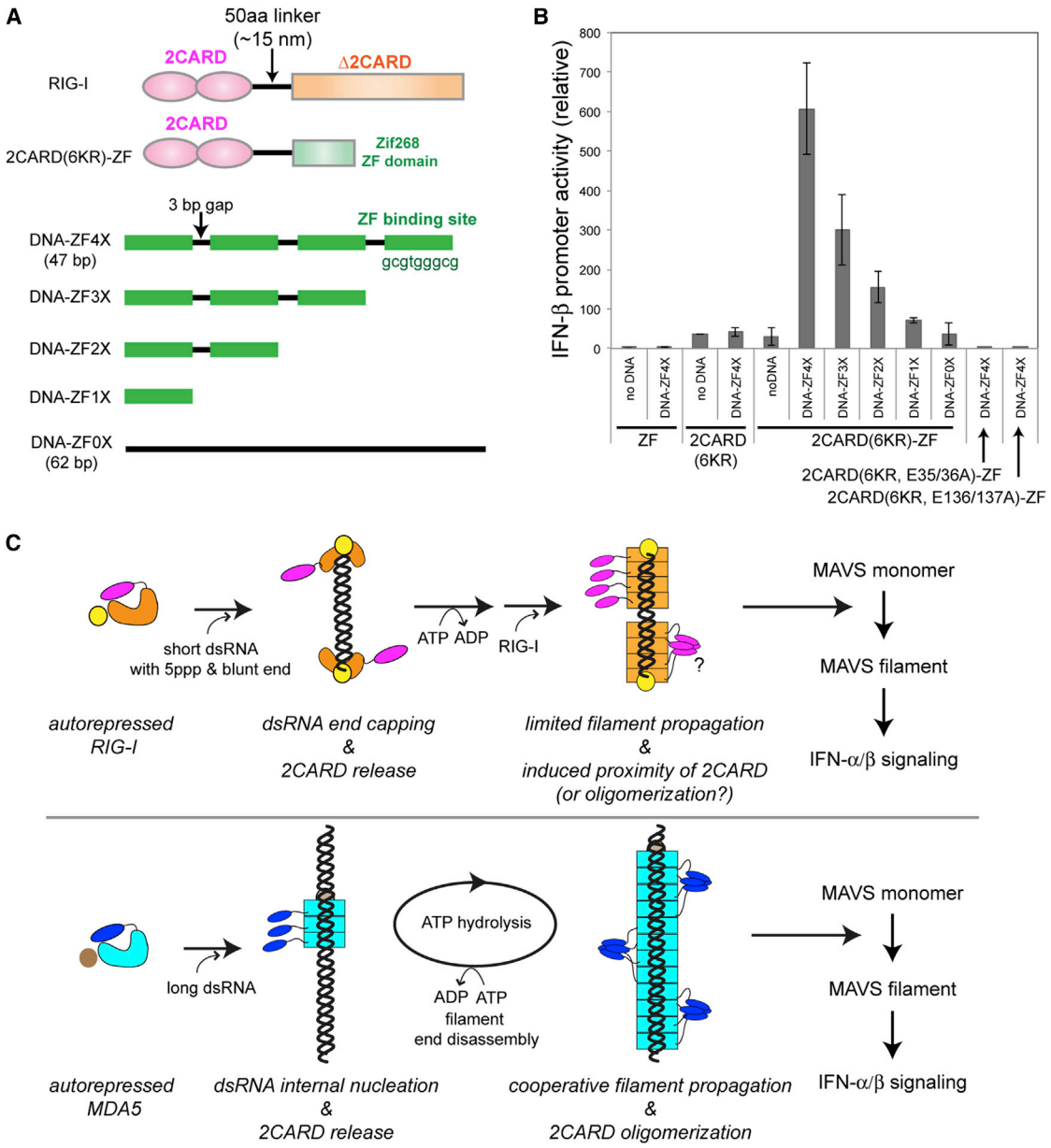

Figure 5. Artificially Induced Proximity of 2CARD Is Sufficient to Activate MAVS Independently of K63-Ub$_n$

(A) Constructs of RIG-I 2CARD(6KR)-ZF and DNA oligonucleotides containing 0–4 copies of tandem ZF-binding sites.

(B) IFN-β reporter assay of RIG-I 2CARD(6KR)-ZF with and without DNA containing 0–4 copies of tandem ZF-binding sites (mean ± SD, n = 3).

(C) A model of filament formation and K63-Ub$_n$-independent IFN-β signal activation by RIG-I and MDA5. RIG-I filaments are formed from dsRNA ends to interiors, possibly by sequential recruitment of individual RIG-I molecules to the dsRNA ends and their ATP-driven translocation to the dsRNA interior. A growing filament may encounter another filament approaching from the opposite end or internally bound RIG-I molecules, which would limit efficient propagation of the filament. Filament formation would induce proximity of 2CARD domains, which may promote their oligomerization and, in turn, stimulate MAVS filament formation. ATP-driven RIG-I filament assembly from dsRNA ends to the interior is in contrast to ATP-independent internal nucleation and filament assembly and ATP-driven end disassembly of the MDA5 filament. However, proximity or oligomerization of 2CARD within the filament to stimulate MAVS could be a shared mechanism between the RIG-I and MDA5 filaments. The number of 2CARD domains constituting an oligomer within the MDA5 filament is hypothetical.

compared with short dsRNA at an equivalent mass concentration, which limits recruitment of RIG-I for filament assembly (Figure 1H). In addition, RIG-I filaments propagate with limited cooperativity (Figures 1E and 1H), which further results in less-efficient coating and recognition of longer dsRNA.

MDA5 also forms filaments along dsRNA to induce signal activation through MAVS, suggesting a common mechanism for both RIG-I and MDA5 in which the duplex RNA structure is utilized as a scaffold for receptor oligomerization. However, unlike RIG-I filaments, MDA5 nucleates within the duplex

interior and forms long, continuous filaments through a highly cooperative process in the absence of ATP (Figure 5C). ATP hydrolysis instead triggers end disassembly of the MDA5 filament, which decreases the filament stability on short dsRNA (Peisley et al., 2012), allowing preferential recognition of long dsRNA (>~1–2 kb) generated during replication of positive strand viruses (Feng et al., 2012; Kato et al., 2011; Triantafilou et al., 2012). Thus, RIG-I and MDA5 utilize the same domain architecture and similar higher-order assemblies, yet perform divergent functions in viral recognition through distinct filament assembly and disassembly mechanisms.

EXPERIMENTAL PROCEDURES

Detailed experimental procedures are provided in the Supplemental Experimental Procedures.

Electrophoretic Mobility Shift Assay

Unless mentioned otherwise, EMSA was performed by incubating dsRNA (1 μg/ml) and RIG-I (1 μM or indicated amount) in buffer A (20 mM HEPES (pH 7.5), 150 mM NaCl, 1.5 mM $MgCl_2$, and 2 mM dithiothreitol [DTT]) in the presence and absence of 1 mM ATP or ATP analogs for 10 min at room temperature (RT), and the complex was analyzed on Bis-Tris NativePAGE (Life Technologies). Gels were stained with SYBR Gold (Life Technologies), and fluorescent gel images were recorded using an FLA 9000 scanner (Fujifilm) and analyzed with MultiGauge (Fujifilm).

Electron Microscopy

RIG-I (0.2 μM) was incubated with dsRNA (0.66 μg/ml regardless of its length) in buffer A with 1 mM ATP for 10 min at RT. ATP hydrolysis was quenched with 2 mM ADP•AlF_x on ice (Figure S1A). See Figure S1B for filaments without quenching. ADP•AlF_x was prepared by mixing ADP, $AlCl_3$, and NaF in a molar ratio of 1:1:3. Prepared filaments were adsorbed to carbon-coated grids (Ted Pella, Inc.) and stained with uranyl formate as described (Ohi et al., 2004). Images were collected using a Phillips CM10 and Tecnai T12 electron microscope (FEI). See Supplemental Experimental Procedures for details.

MAVS Filament Formation Assay

The MAVS filament formation assay was performed as previously reported (Wu et al., 2013). Refolded, Alexa 647-labeled monomer of CARD-S was prepared as described in the Supplemental Experimental Procedures. Monomeric CARD-S is functional, as it can efficiently extend CARD-S filament seeds (Wu et al., 2013). In the absence of external stimuli or seed filaments, refolded MAVS CARD remains as a stable monomer over 24 hr, after which it spontaneously forms prion-like filaments over the course of days. Thus, all assays involving MAVS filament formation were performed within 6 hr after refolding. Labeled, monomeric MAVS CARD-S (CARD-S*, 10 μM) was incubated with various combinations of RIG-I (1 μM), dsRNA (5.4 μg/ml regardless of its length, equivalent to 80 nM 112 bp dsRNA), ATP or ATP analog (2 mM), and K63-Ub_n (0.18 mg/ml, equivalent to 24 μM monomeric Ub) in buffer A for 1 hr at RT prior to analysis by Bis-Tris NativePAGE (Life Technologies) or by EM. Fluorescent gel images were recorded using an FLA 9000 scanner (Fujifilm).

SUPPLEMENTAL INFORMATION

Supplemental Information includes Supplemental Experimental Procedures and four figures and can be found with this article online at http://dx.doi.org/10.1016/j.molcel.2013.07.024.

ACKNOWLEDGMENTS

B.W. is a GSK fellow. T.W. is an Investigator with the Howard Hughes Medical Institute. S.H. is a recipient of a Pew Scholarship, Massachusetts Life Science Center New Investigator Award, and Milton Foundation Fund.

Received: April 22, 2013
Revised: June 27, 2013
Accepted: July 25, 2013
Published: August 29, 2013

REFERENCES

Bamming, D., and Horvath, C.M. (2009). Regulation of signal transduction by enzymatically inactive antiviral RNA helicase proteins MDA5, RIG-I, and LGP2. J. Biol. Chem. *284*, 9700–9712.

Baum, A., Sachidanandam, R., and García-Sastre, A. (2010). Preference of RIG-I for short viral RNA molecules in infected cells revealed by next-generation sequencing. Proc. Natl. Acad. Sci. USA *107*, 16303–16308.

Berke, I.C., and Modis, Y. (2012). MDA5 cooperatively forms dimers and ATP-sensitive filaments upon binding double-stranded RNA. EMBO J. *31*, 1714–1726.

Berke, I.C., Yu, X., Modis, Y., and Egelman, E.H. (2012). MDA5 assembles into a polar helical filament on dsRNA. Proc. Natl. Acad. Sci. USA *109*, 18437–18441.

Binder, M., Eberle, F., Seitz, S., Mücke, N., Hüber, C.M., Kiani, N., Kaderali, L., Lohmann, V., Dalpke, A., and Bartenschlager, R. (2011). Molecular mechanism of signal perception and integration by the innate immune sensor retinoic acid-inducible gene-I (RIG-I). J. Biol. Chem. *286*, 27278–27287.

Davis, D.R. (1998). Biophysical and conformational properties of modified nucleosides in RNA (Washington, D.C.: American Society for Microbiology).

Feng, Q., Hato, S.V., Langereis, M.A., Zoll, J., Virgen-Slane, R., Peisley, A., Hur, S., Semler, B.L., van Rij, R.P., and van Kuppeveld, F.J.M. (2012). MDA5 detects the double-stranded RNA replicative form in picornavirus-infected cells. Cell Rep *2*, 1187–1196.

Gack, M.U., Shin, Y.C., Joo, C.H., Urano, T., Liang, C., Sun, L., Takeuchi, O., Akira, S., Chen, Z., Inoue, S., and Jung, J.U. (2007). TRIM25 RING-finger E3 ubiquitin ligase is essential for RIG-I-mediated antiviral activity. Nature *446*, 916–920.

Horowitz, S., Horowitz, A., Nilsen, T.W., Munns, T.W., and Rottman, F.M. (1984). Mapping of N6-methyladenosine residues in bovine prolactin mRNA. Proc. Natl. Acad. Sci. USA *81*, 5667–5671.

Hou, F., Sun, L., Zheng, H., Skaug, B., Jiang, Q.X., and Chen, Z.J. (2011). MAVS forms functional prion-like aggregates to activate and propagate antiviral innate immune response. Cell *146*, 448–461.

Jamieson, A.C., Wang, H., and Kim, S.-H. (1996). A zinc finger directory for high-affinity DNA recognition. Proc. Natl. Acad. Sci. USA *93*, 12834–12839.

Jiang, F., Ramanathan, A., Miller, M.T., Tang, G.-Q., Gale, M., Jr., Patel, S.S., and Marcotrigiano, J. (2011). Structural basis of RNA recognition and activation by innate immune receptor RIG-I. Nature *479*, 423–427.

Jiang, X., Kinch, L.N., Brautigam, C.A., Chen, X., Du, F., Grishin, N.V., and Chen, Z.J. (2012). Ubiquitin-induced oligomerization of the RNA sensors RIG-I and MDA5 activates antiviral innate immune response. Immunity *36*, 959–973.

Kato, H., Takeuchi, O., Mikamo-Satoh, E., Hirai, R., Kawai, T., Matsushita, K., Hiiragi, A., Dermody, T.S., Fujita, T., and Akira, S. (2008). Length-dependent recognition of double-stranded ribonucleic acids by retinoic acid-inducible gene-I and melanoma differentiation-associated gene 5. J. Exp. Med. *205*, 1601–1610.

Kato, H., Takahasi, K., and Fujita, T. (2011). RIG-I-like receptors: cytoplasmic sensors for non-self RNA. Immunol. Rev. *243*, 91–98.

Kowalinski, E., Lunardi, T., McCarthy, A.A., Louber, J., Brunel, J., Grigorov, B., Gerlier, D., and Cusack, S. (2011). Structural basis for the activation of innate immune pattern-recognition receptor RIG-I by viral RNA. Cell *147*, 423–435.

Lazzarini, R.A., Keene, J.D., and Schubert, M. (1981). The origins of defective interfering particles of the negative-strand RNA viruses. Cell *26*, 145–154.

Leaver-Fay, A., Tyka, M., Lewis, S.M., Lange, O.F., Thompson, J., Jacak, R., Kaufman, K., Renfrew, P.D., Smith, C.A., Sheffler, W., et al. (2011). ROSETTA3: an object-oriented software suite for the simulation and design of macromolecules. Methods Enzymol. *487*, 545–574.

Lu, C., Xu, H., Ranjith-Kumar, C.T., Brooks, M.T., Hou, T.Y., Hu, F., Herr, A.B., Strong, R.K., Kao, C.C., and Li, P. (2010). The structural basis of 5′ triphosphate double-stranded RNA recognition by RIG-I C-terminal domain. Structure *18*, 1032–1043.

Luo, D., Ding, S.C., Vela, A., Kohlway, A., Lindenbach, B.D., and Pyle, A.M. (2011). Structural insights into RNA recognition by RIG-I. Cell *147*, 409–422.

Makeyev, E.V., and Grimes, J.M. (2004). RNA-dependent RNA polymerases of dsRNA bacteriophages. Virus Res. *101*, 45–55.

Myong, S., Cui, S., Cornish, P.V., Kirchhofer, A., Gack, M.U., Jung, J.U., Hopfner, K.-P., and Ha, T. (2009). Cytosolic viral sensor RIG-I is a 5′-triphosphate-dependent translocase on double-stranded RNA. Science *323*, 1070–1074.

Ohi, M., Li, Y., Cheng, Y., and Walz, T. (2004). Negative staining and image classification - powerful tools in modern electron microscopy. Biol. Proced. Online *6*, 23–34.

Peisley, A., Lin, C., Wu, B., Orme-Johnson, M., Liu, M., Walz, T., and Hur, S. (2011). Cooperative assembly and dynamic disassembly of MDA5 filaments for viral dsRNA recognition. Proc. Natl. Acad. Sci. USA *108*, 21010–21015.

Peisley, A., Jo, M.H., Lin, C., Wu, B., Orme-Johnson, M., Walz, T., Hohng, S., and Hur, S. (2012). Kinetic mechanism for viral dsRNA length discrimination by MDA5 filaments. Proc. Natl. Acad. Sci. USA *109*, E3340–E3349.

Schlee, M., Roth, A., Hornung, V., Hagmann, C.A., Wimmenauer, V., Barchet, W., Coch, C., Janke, M., Mihailovic, A., Wardle, G., et al. (2009). Recognition of 5′ triphosphate by RIG-I helicase requires short blunt double-stranded RNA as contained in panhandle of negative-strand virus. Immunity *31*, 25–34.

Sekellick, M.J., and Marcus, P.I. (1982). Interferon induction by viruses. VIII. Vesicular stomatitis virus: [+/-]DI-011 particles induce interferon in the absence of standard virions. Virology *117*, 280–285.

Shigemoto, T., Kageyama, M., Hirai, R., Zheng, J.P., Yoneyama, M., and Fujita, T. (2009). Identification of loss of function mutations in human genes encoding RIG-I and MDA5: implications for resistance to type I diabetes. J. Biol. Chem. *284*, 13348–13354.

Strahle, L., Garcin, D., and Kolakofsky, D. (2006). Sendai virus defective-interfering genomes and the activation of interferon-beta. Virology *351*, 101–111.

Triantafilou, K., Vakakis, E., Kar, S., Richer, E., Evans, G.L., and Triantafilou, M. (2012). Visualisation of direct interaction of MDA5 and the dsRNA replicative intermediate form of positive strand RNA viruses. J. Cell Sci. *125*, 4761–4769.

Wang, Y., Ludwig, J., Schuberth, C., Goldeck, M., Schlee, M., Li, H., Juranek, S., Sheng, G., Micura, R., Tuschl, T., et al. (2010). Structural and functional insights into 5′-ppp RNA pattern recognition by the innate immune receptor RIG-I. Nat. Struct. Mol. Biol. *17*, 781–787.

Wu, B., Peisley, A., Richards, C., Yao, H., Zeng, X., Lin, C., Chu, F., Walz, T., and Hur, S. (2013). Structural basis for dsRNA recognition, filament formation, and antiviral signal activation by MDA5. Cell *152*, 276–289.

Yoneyama, M., Kikuchi, M., Natsukawa, T., Shinobu, N., Imaizumi, T., Miyagishi, M., Taira, K., Akira, S., and Fujita, T. (2004). The RNA helicase RIG-I has an essential function in double-stranded RNA-induced innate antiviral responses. Nat. Immunol. *5*, 730–737.

Zeng, W., Sun, L., Jiang, X., Chen, X., Hou, F., Adhikari, A., Xu, M., and Chen, Z.J. (2010). Reconstitution of the RIG-I pathway reveals a signaling role of unanchored polyubiquitin chains in innate immunity. Cell *141*, 315–330.